Arch. Min. Sci. **63** (2018), 2, 353-382

Electronic version (in color) of this paper is available: http://mining.archives.pl

DOI 10.24425/122452

QINGFA CHEN*,**#, TINGCHANG YIN*,**, WENJING NIU**,***

REPLACING RQD AND DISCONTINUITY SPACING WITH THE MODIFIED BLOCKINESS INDEX IN THE ROCK MASS RATING SYSTEM

ZASTĄPIENIE KLASYFIKACJI JAKOŚCI SKAŁ (RQD) I ODLEGŁOŚCI POMIĘDZY NIECIĄGŁOŚCIAMI SKAŁ ZMODYFIKOWANYM WSPÓŁCZYNNIKIEM OPISUJĄCYM STRUKTURĘ BLOKOWĄ WARSTW SKALNYCH W SYSTEMIE OCENY STANU GÓROTWORU

The evaluation accuracies of rock mass structures based on the ratings of the Rock Quality Designation (RQD) and discontinuity spacing (*S*) in the Rock Mass Rating (RMR) system are very limited due to the inherent restrictions of RQD and *S*. This study presents an improvement that replaces these two parameters with the modified blockiness index (B_z) in the RMR system. Before proceeding with this replacement, it is necessary for theoretical model building to make an assumption that the discontinuity network contains three sets of mutually orthogonal disc-shaped discontinuities with the same diameter and spacing of discontinuities. Then, a total of 35 types of theoretical DFN (Discrete Fracture Network) models possessing the different structures were built based on the International Society for Rock Mechanics (ISRM) discontinuity classification (ISRM, 1978). In addition, the RQD values of each model were measured by setting the scanlines in the models, and the B_z values were computed following the modified blockiness evaluation method. Correlations between the three indices (i.e., B_z, RQD and *S*) were explored, and the reliability of the substitution was subsequently verified. Finally, RMR systems based on the proposed method and the standard approach were applied to real cases, and comparisons between the two methods were performed. This study reveals that RQD is well correlated with *S* but is difficult to relate to the discontinuity diameter (*D*), and B_z has a good correlation with RQD/*S*. Additionally, the ratings of RQD and *S* are always far from the actual rock mass structure, and the B_z ratings are found to give better characterizations of rock mass structures. This substitution in the RMR system was found to be acceptable and practical.

Keywords: Rock Quality Designation; Discontinuity spacing; Modified blockiness index; Substitution; Rock Mass Rating

* COLLEGE OF RESOURCES, ENVIRONMENT AND MATERIALS, GUANGXI UNIVERSITY, NANNING, GUANGXI, 530004, PR CHINA

** STATE KEY LABORATORY OF GEOMECHANICS AND GEOTECHNICAL ENGINEERING, INSTITUTE OF ROCK AND SOIL MECHANICS, CHINESE ACADEMY OF SCIENCES, WUHAN, 430071, PR CHINA

*** SCHOOL OF RESOURCES AND CIVIL ENGINEERING, NORTHEASTERN UNIVERSITY, SHENYANG, 110819, PR CHINA

\# Corresponding author: gxumining@163.com

Dokładność oceny struktury górotworu w oparciu o określenie jakości skał oraz odległości pomiędzy kolejnymi nieciągłościami (*S*) w systemie oceny stanu górotworu (RMR-Rock Mass Rating) jest mocno ograniczona z powodu ograniczeń wbudowanych w samą strukturę modelu RQD i w procedury obliczania odległości pomiędzy nieciągłościami. W niniejszej pracy zaproponowano ulepszone rozwiązanie zakładające zastąpienie powyższych dwóch parametrów przez jeden wskaźnik oceny struktury blokowej (B_z) w systemie RMR. Jednakże przed zastąpieniem wskaźników konieczne okazało się opracowanie modelu teoretycznego opartego na założeniu że sieć nieciągłości zawiera trzy zbiory wzajemnie ortogonalnych nieciągłości w kształcie dysków, mających tę samą średnicę i zlokalizowanych w równych odstępach. Następnie opracowano w sumie 35 typów teoretycznych dyskretnych modeli nieciągłości DFN (Discrete Fracture Network) o różnych strukturach w oparciu o klasyfikację nieciągłości określoną przez International Society for Rock Mechanics (ISRM, 1978). Ponadto, wartości RQD dla każdego z modeli zostały zmierzone poprzez odpowiednie ustawienie linii wybierania w modelu, zaś wartości B_z obliczono w oparciu o zmodyfikowaną metodę oceny struktury blokowej. Badano wzajemne korelacje pomiędzy trzema wskaźnikami (B_z, RQD, *S*), badano także wiarygodność modeli po podstawieniu. W etapie końcowym, system RMR oparty na zaproponowanej metodzie i podejściu standardowym został zastosowany do analizy rzeczywistych przypadków w celu porównania wyników uzyskanych w oparciu o powyższe dwie metody. Wyniki wskazały wysoki stopień korelacji wielkości RQD i *S*, choć trudno znaleźć korelacje pomiędzy RQD a średnicą nieciągłości (*D*). Stwierdzono także wysoki stopień korelacji pomiędzy wartościami RQD i *S*. Ponadto, stwierdzono że wielkości RQD i *S* nie opisują dokładnie rzeczywistej struktury górotworu, zaś ocena oparta na wskaźniku B_z wydaje się lepiej charakteryzować jego strukturę. Podstawienie tego parametru do systemu klasyfikacji RMR wydaje się więc akceptowalne i uzasadnione praktycznie.

Słowa kluczowe: system określenia jakości skał, odstępy pomiędzy nieciągłościami, zmodyfikowany wskaźnik opisujący strukturę blokową górotworu, zamiana współczynników, system klasyfikacji skał

Abbreviations and nomenclatures

B	–	Block percentage,
B_z	–	The modified blockiness evaluation method,
$C_{v\text{-RQD}}$	–	The coefficient of variation of RQD values,
D	–	Discontinuity diameter,
d_3	–	Three-dimensional discontinuity density,
ISRM	–	International Society for Rock Mechanics,
J_v	–	Volumetric joint count,
K_v	–	Chinese rating of the intactness index of rock mass,
RMDI	–	Rock Mass Integrity Index,
RMR	–	Rock Mass Rating,
RQD	–	Rock Quality Designation,
S	–	Discontinuity spacing,
Unexposed blocks	–	The blocks fully enclosed by discontinuities within a rock mass.

1. Introduction

In 1973, the Rock Mass Rating (RMR) system (Bieniawski, 1973; 1989), a geomechanical rock mass classification, was first developed to estimate rock mass properties and as a predesign tool in the preliminary stage of mining and civil engineering projects. The latest version of the RMR system is composed of six input parameters, including intact rock uniaxial compressive strength, Rock Quality Designation (RQD), discontinuity spacing (*S*), discontinuity condition,

groundwater condition and discontinuity orientation. The RMR value is the sum of the scores of these six input parameters, and a high score indicates a good rock mass quality. Owing to the easy execution, less input and comprehensive consideration, the RMR system is widely used to evaluate the geomechanical features and stability of engineering rock mass and to determine the tunnel support type worldwide (Aksoy, 2008; Lowson & Bieniawski, 2013). Meanwhile, a number of further studies on the RMR system have been conducted, including improvements of the RMR model (Sen, 2003; Sereshki et al., 2010; Jalalifar et al., 2011, 2014; Nikafshan et al., 2015; Mutlu, 2017), the estimations of rock mass properties based on the RMR system (Liu et al., 1999; González et al., 2006; Palmstrom, 2009; Khademi et al., 2010; Justo et al., 2010; Paul et al., 2012; Jain et al., 2016; Chen et al., 2017), the characterizations of RMR spatial heterogeneity (Ferrari et al., 2014; Pinheiro et al., 2016) and several specialized rock mass classifications relating to the RMR system (Romana, 1993; Atr, 2001; Liu et al., 2014; Warren et al., 2016).

The RMR system has been revised twice by Bieniawski since its introduction. Subsequently, its limitations have been highlighted by many researchers, including that its qualitative parameters are mainly determined by expert's experience, its failure to distinguish heterogeneous rock masses and difficulty of applying the system in weak rock mass. However, the above-mentioned limitations have been overcome with the development of the RMR system (Aksoy, 2008; Wang and Li et al., 2013; Warren, 2016).

In recent years, many researchers, including Bieniawski, have recognized a critical restriction in the RMR system, that the reliability of the RQD and *S* ratings are questionable (Lowson and Bieniawski, 2013; Pells and Bieniawski et al., 2017). The inherent limitations of RQD and *S* were summarized by a previous study (Palmstrom, 2005), and include the following:

- The RQD method does not consider the effects of block scales, and completely different RQD values are measured in the same rock mass due to the different directions of boreholes;
- *S* can be easily measured when one distinct discontinuity set occurs; however, it is difficult to determine *S* when more than one discontinuity set exists;
- RQD has a good relation with *S*, thus the combined use of RQD and *S* breaks the rule (Wang, 2007; Hoseinie et al., 2008) that equivalent parameters should be avoided; and
- The values of RQD and *S* are based on one-dimensional discontinuity data, and it is obviously limited that they are both used to evaluate the three-dimensional structure of rock mass.

In addition, Pells and Bieniawski et al. (2017) reported several cases of abuse and inherent limitations of RQD and suggested that the incorporation of RQD into the rock mass classification is no longer necessary. Therefore, the combined use of RQD and *S* should be replaced, and a more suitable and accurate characterization of rock mass structures should be used in the RMR system.

Some researchers have investigated the rock mass structure and presented several measurements for the degree of rock mass fracturing. Chen (1979) presented the concept of a two-dimensional blockiness modulus that characterizes the rock mass intactness degree based on the two-dimensional discontinuity data measured on rock mass outcrops. Sen and Eissa (1991) proposed the concept of volumetric RQD estimated from the volumetric joint count (*Jv*). Palmstrom (2005) developed a correlation between *Jv* and block sizes within rock masses. Wang et al. (2010) presented a new method, the Rock Mass Integrity Index (RMDI), to describe the rock mass intactness degree based on borehole camera technology. Xia and Wang et al. (2013, 2015) investigated the rock mass blocks of the engineering projects in Wudongde and the Three

Gorges, China, and measured the blockiness level and three-dimensional blockiness modulus of the blocks. However, some limitations still exist in these measurements: discontinuities are regarded as infinite planes when *Jv* is computed (Li et al., 2009), two-dimensional modulus is imprecise (Wang, 2013), RMDI cannot reflect rock mass heterogeneity (Li et al., 2017), and the effect of block dimensions is neglected by some measurements, such as *Jv* (Hoek et al., 2013) and the current blockiness evaluation method (Niu, 2017). The authors have investigated the blockiness evaluation method, and considering the influence of block dimensions on rock mass integrity, the authors also developed the modified blockiness index (B_z), which assesses the rock mass intactness degree more precisely (Niu, 2017). Therefore, this study attempts to substitute B_z for RQD and *S* in the RMR system. To support its reliability, a total of 35 types of theoretical DFN (Discrete Fracture Network) models, which contain three sets of mutually orthogonal disc-shaped discontinuities and have the same diameter and spacing of discontinuities, were developed based on the discontinuity classification of the International Society for Rock Mechanics (ISRM) (ISRM, 1978). Based on the B_z and RQD values of these models, the correlations between B_z, RQD and *S* were evaluated. By combining this analysis with the theoretical analyses and applications of real cases, the rationality of the substitution was verified. This study may provide a new approach for the improvement of the RMR system.

2. Modified blockiness evaluation method

2.1. Concept of blockiness evaluation method

The blockiness evaluation method was first developed by Xia et al. (2015, 2016) and is used to measure the volumes of the blocks fully enclosed by discontinuities (i.e., unexposed blocks) within rock masses. The block percentage (*B*) is defined as an index for the rock mass blockiness level, which is the percentage of the sum of the volume of unexposed blocks within the rock mass to the total volume of the rock mass. *B* is calculated using the following equation:

$$B = \frac{\sum_{i=1}^{n} v_i}{V} \times 100\% \tag{1}$$

where *V* is the total volume of the rock mass model, v_i is the volume of the block *i* and *n* is the sum of blocks. If *B* is close to 0%, it indicates poorly developed discontinuities in the rock mass and high integrity of the rock mass. On the other hand, when *B* is close to 100%, it indicates an extremely fractured rock mass with well-developed discontinuities. The current blockiness classification is shown in Table 1.

TABLE 1

Classification of the blockiness level (Liu, 2010)

Block percentage (%)	Description
$0 \le B \le 10$	Non-blockiness
$10 \le B \le 30$	Slight-blockiness
$30 \le B \le 60$	Moderate-blockiness
$60 \le B \le 100$	Blockiness

2.2. Modified blockiness index (B_z)

The current blockiness index has some shortcomings, such as its failure to consider the effects of block scales and the unreasonable rating of blockiness. The authors have modified the concept of blockiness and have developed the modified blockiness index (B_z) (Niu, 2017). B_z is computed by using the following equation:

$$B_Z = B_1 + \frac{1}{2}B_2 + \frac{1}{3}B_3 + \frac{1}{4}B_4 + \frac{1}{5}B_5 \tag{2}$$

where B_z (expressed in %) represents the blockiness level of a rock mass, B_1, B_2, B_3, B_4 and B_5 are the block percentages of the volumes in the five intervals (0 ~ 0.008 m^3, 0.008 ~ 0.03 m^3, 0.03 ~ 0.2 m^3, 0.2 ~ 1.0 m^3 and > 1.0 m^3), respectively. The B_z definition considers the small-sized blocks much more and gives them higher weights because the small size blocks are more unfavorable to the engineering construction. Obviously, when fewer small sized blocks occur, the blockiness level is lower, indicating a higher rock mass intactness degree. The new blockiness classification is shown in Table 2.

TABLE 2

New classification of blockiness levels

B_z (%)	Rating	Description	Rating for rock mass intactness degree	Engineering geological description
< 7	I	Non-blockiness rock mass	Integrated	Large discontinuity spacing, good or general cementing status of the discontinuity, integrated or huge thick-layered rock mass.
7 ~ 27	II	Slight-blockiness rock mass	Relatively integrated	Better-developed discontinuities, good or general cementing status of the discontinuity, massive or thick-layered rock mass.
27 ~ 55	III	Moderate-blockiness rock mass	Poorly integrated	Substantially better-developed discontinuities, poor or general cementing status of the discontinuity, massive or mosaic fragmented rock mass.
55 ~ 85	IV	Blockiness rock mass	Relatively fractured	Substantially well-developed discontinuities, poor cementing status of the discontinuity, massive or fragmented rock mass.
≥ 85	V	Serious-blockiness rock mass	Fractured	Substantially disorderly discontinuities, very poor cementing status of the discontinuity, granular rock mass.

The intactness degree of the rock mass is mainly subject to the discontinuity spacing and persistence (Zhang et al., 2009), and the formation of blocks within rock masses are caused by the cross-cutting nature of the different discontinuity sets. Therefore, the B_z value is a quantification of the blockiness degree of a rock mass, and it could be used to assess the intactness degree of a rock mass.

3. Theoretical DFN models of rock masses

3.1. Basic parameters for building the theoretical DFN models

The blockiness level of a rock mass reflects the intactness degree of a rock mass, which is primarily controlled by discontinuity spacing and persistence. Only when three or more sets of discontinuities intersect can the blocks occur within a rock mass, and the changes of discontinuity orientations have little influence on the blockiness level of rock mass (Zhang et al., 2009), hence, the discontinuity orientations were fixed in some studies (Yang et al., 1998; Ruf et al., 1998; Kuszmaul, 1999; Palmstrom, 2005; Xia et al., 2016; Li et al., 2016). In addition, yet, very little research has integrated the discontinuity spacing and persistence to describe the rock mass structure and subsequently incorporate it into the rock mass classification. Therefore, in this study, the reliability of substituting B_z (a quantitative index of rock mass blockiness level) for the RQD and S in the RMR system was investigated.

To remove the influences of the random distributions of discontinuity sizes and orientations, and to simplify the analytical models, the theoretical three-dimensional discontinuity networks of rock mass were employed, which contain three mutually orthogonal disc-shaped discontinuity sets that have the same diameter and spacing of discontinuities. The discontinuity diameter (D) is calculated by (Shi, 2006):

$$D = \frac{4l}{\pi} \tag{3}$$

where l is the discontinuity trace.

The discontinuity classification suggested by the ISRM divides the discontinuity diameters and the discontinuity spacing into five classes and seven classes, respectively. To consider the influences of the discontinuities of different sizes and densities on rock mass integrities, twelve typical values were chosen from each class, including five D values and seven S values, as shown in Tables 3 and 4, and subsequently thirty-five types of DFN models that contain discontinuities of different sizes and densities were built by GeneralBlock (a computer program written by Yu) (Yu, 2009; Wang, 2013; Xia et al., 2015, 2016) (Fig. 1). The relation between the three-dimensional density of one discontinuity set (d_3), D and S is:

$$d_3 = \frac{4}{\pi E(D^2)S} \tag{4}$$

where d_3 is the number of discontinuities within a unit volume of the rock mass, $E(D^2)$ is the mean value of the squared discontinuity diameter. All the models' d_3 values are computed by Eq. (4), as shown in Table 5.

TABLE 3

Classification of discontinuity persistence of rock mass (ISRM, 1978)

Description	Very low	Low	Medium	High	Very high
D (m)	< 1	1 ~ 3	3 ~ 10	10 ~ 20	> 20
Chosen typical value (m)	1	3	10	20	40

TABLE 4

Classification of discontinuity spacing of rock mass (ISRM, 1978)

Description	Extremely close	Very close	Close	Moderate	Wide	Very wide	Extremely wide
S (m)	< 0.02	0.02 ~ 0.06	0.06 ~ 0.2	0.2 ~ 0.6	0.6 ~ 2	2 ~ 6	> 6
Chosen typical value (m)	0.02	0.04	0.13	0.4	1.3	4	6

TABLE 5

Three-dimensional discontinuity densities of thirty-five models

D (m)	S (m)						
	0.02	**0.04**	**0.13**	**0.4**	**1.3**	**4**	**6**
40	0.1194	0.0597	0.0183	0.006	0.0018	0.0006	0.0003
20	0.4776	0.2388	0.0735	0.024	0.0072	0.0024	0.0015
10	1.9107	0.9555	0.294	0.0954	0.0294	0.0096	0.0063
3	21.2313	10.6158	3.2664	1.0617	0.3267	0.1062	0.0708
1	190.986	95.493	29.3826	9.5493	2.9382	0.9549	0.6366

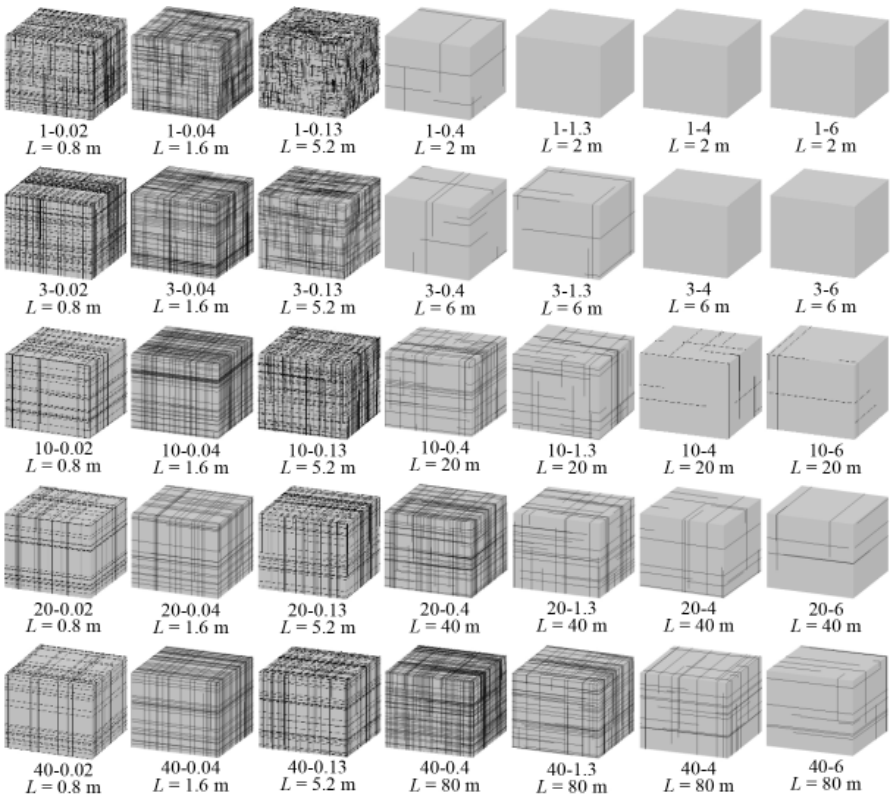

Fig. 1. Three-dimensional discontinuity systems of thirty-five models (note that the subtitle of "1-0.02" indicates that the D is 1 m and the S is 0.02 m and is similar for the remaining subtitles of this figure, and L denotes the side length of the model)

3.2. Building theoretical DFN models of rock masses

To satisfy the requirements of Representative Elementary Volume (REV), the side length of the models is between 20 and 50 times the *S* when the *S* is in the range from extremely close to close, and the length is approximately 0.3-4 times that of the *D* if the *S* ranges between the moderate to the extremely wide categories (Niu, 2017). Thirty-five types of DFN models were built by GeneralBlock, as shown in Fig. 1. Note that the practical applications of the blockiness evaluation method are presented in (Wang, 2013; Xia et al., 2015). In this study, 35 types of theoretical models are established to evaluate the correlations between RQD, *S* and B_z and to discuss the reliability of replacing RQD and *S* with B_z in normal and extreme conditions.

4. Computing RQD and *Bz*

4.1. Calculation of RQD

The RQD values were measured by setting the scanlines in the models, i.e., using scanlines to simulated boreholes. To avoid direction bias, three sections were obtained by the model dimidiation in the ***X***, ***Y*** and ***Z*** directions, and then scanlines through the geometrical center of

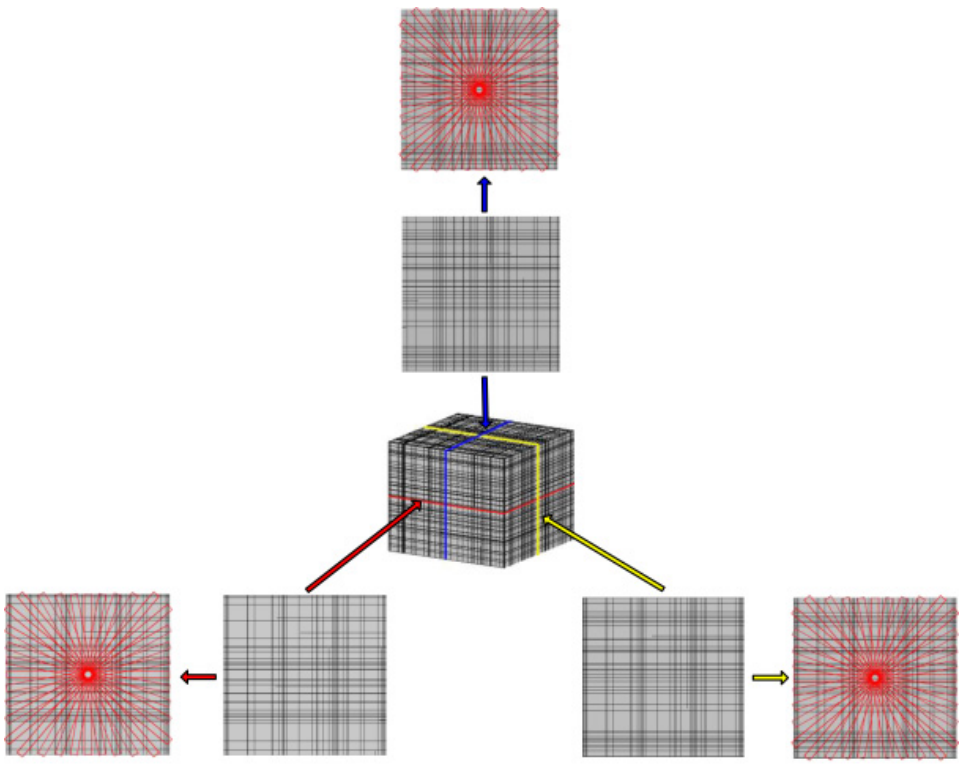

Fig. 2. Setting scanlines in a model

the sections were set every 10 degrees. Therefore, eighteen scanlines were set in a section, and there are fifty-four scanlines, in total, in a model, as shown in Fig. 2. All the RQD values of the 35 models are depicted in Fig. 3, and it shows the following:

(i) When the *D* is fixed, the RQD values markedly increase with the increase in *S*. When *S* is in the range from extremely close to close, the heterogeneities of the RQD values of all the models are significant, which indicates that, in such a condition, borehole directions have great effects on the RQD values; however, if *S* is in the range from moderate to extremely wide, the RQD values of all the models tend to plateau, which means that the influences of borehole directions on the RQD values are reduced as the *S* values continue to increase.

(ii) When *S* is fixed, the RQD values have a poor correlation with *D*. In the condition of a fixed *S* value in the range from extremely close to moderate and with variable *D* values, the RQD values vary markedly; under the conditions of an unchanged *S* value in the range from wide to extremely wide and with variable *D* values, all the RQD values are close to 100%.

RQD is well correlated with *S* and has a poor correlation with *D*. This conclusion is similar to the findings of previous studies (Priest, 1993; Palmstrom, 2005).

4.2. Calculation of *Bz*

The volumes of unexposed blocks within the models were calculated by GeneralBlock, and then, the B_z values were computed by Eq. (2). The B_z values of all the models are shown in Table 6. There are some correlations between B_z, *D* and *S*. As seen in Table 6, when the *D* is fixed, decreasing B_z values are experienced with the increase in *S*; if *S* is fixed, the B_z values are reduced with the reduction of *D*.

TABLE 6

All models' B_z values and classifications

***D* (m)**	***S* (m)**						
	0.02	**0.04**	**0.13**	**0.40**	**1.30**	**4.00**	**6.00**
40	93.7571	91.4286	61.2567	27.5231	17.5350	10.5002	0.3650
	V	V	IV	III	II	II	I
20	91.0728	87.5613	44.6782	23.9566	13.5002	0.3186	0.0307
	V	V	III	II	II	I	I
10	90.2910	87.2045	44.0021	20.9621	4.6818	0.0573	0.0012
	V	V	III	II	I	I	I
3	88.9321	86.0180	43.8025	7.9657	0.1070	1.20E-8	1.78E-10
	V	V	III	II	I	I	I
1	87.9759	84.3504	18.2843	0.1110	5.13E-5	1.03E-7	1.74E-9
	V	IV	III	I	I	I	I

The block volume curve, an interpretation of the probability and distribution of blocks within a rock mass (Elmouttie & Poropat, 2012; Stavropoulou, 2014; Ruiz-Carulla et al., 2015), is employed to analyze the differences of block distributions and scales between various models

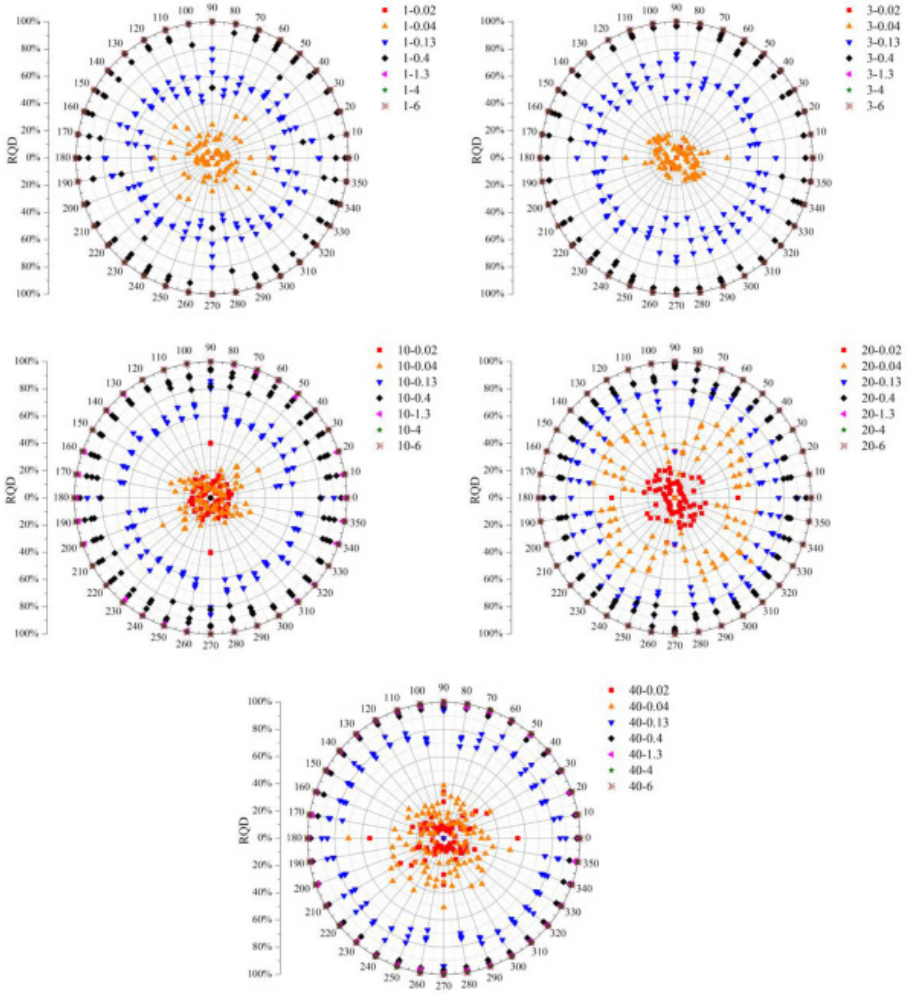

(a) RQD values in the conditions of variable *S* and fixed *D*

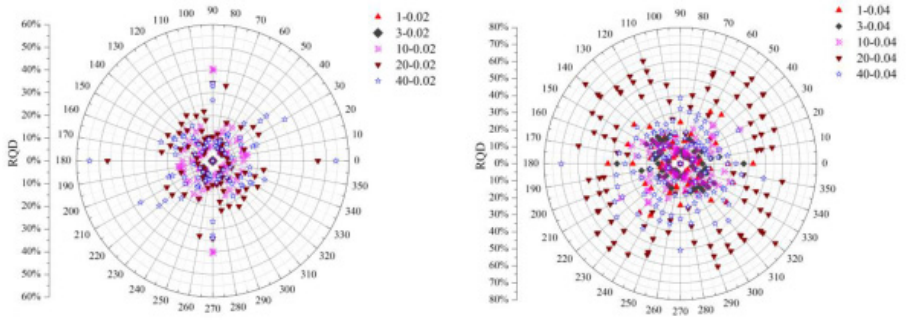

Fig. 3. All the models' RQD values (note that in this figure, the "1-0.02" means that the model's discontinuity diameter and spacing are 1 m and 0.02 m, respectively, and is similar for the others of this figure)

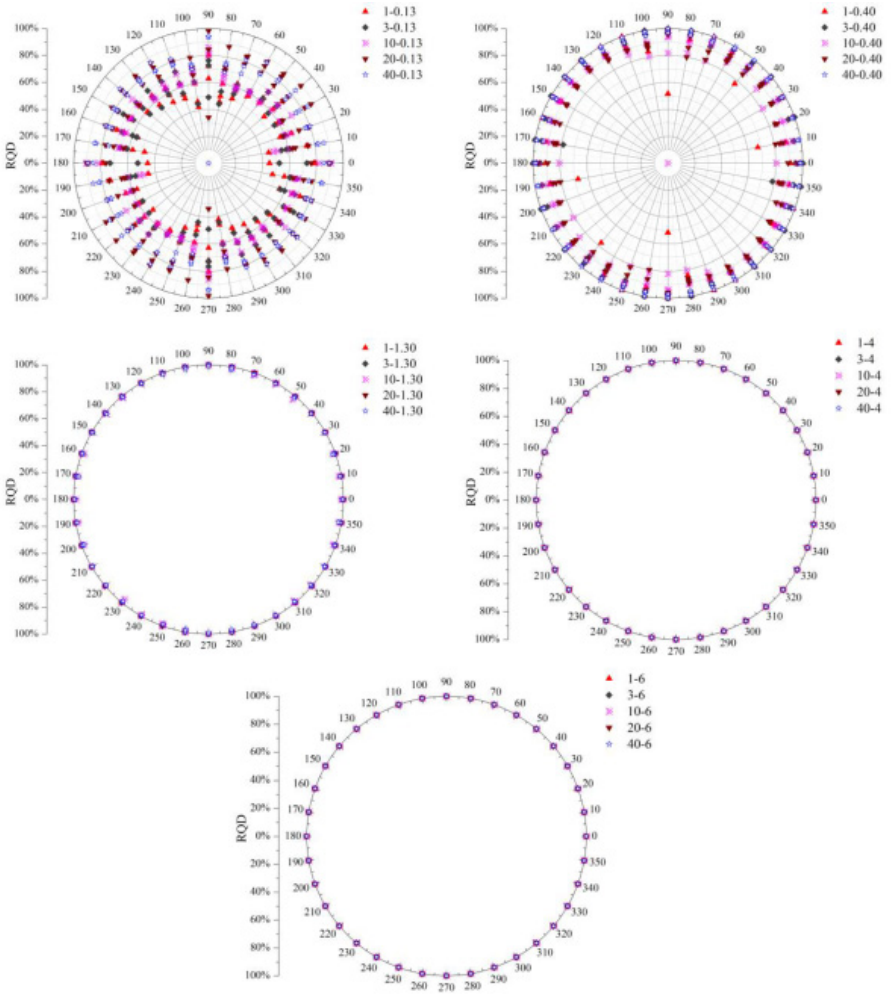

(b) RQD values in the conditions of variable *D* and fixed *S*

Fig. 3. All the models' RQD values (note that in this figure, the "1-0.02" means that the model's discontinuity diameter and spacing are 1 m and 0.02 m, respectively, and is similar for the others of this figure)

in this study, and the block volume curves of 35 types of models are depicted in Fig. 4. The figure shows that when the *D* values are variable, the block volumes are also different. For example, if the *D* value is fixed at 1 m or 40 m, the blocks within the rock mass are of a scale of 10^{-2} m^3 or 10^3 m^3, respectively. Therefore, the block sizes are relative within a rock mass. In the condition of a fixed *D*, the closer the *S* values are, the larger the numbers of relatively small blocks are, and vice versa. Additionally, the conditions that occur with relatively large blocks are different. For example, when the *D* value is fixed at a small value (e.g., 1 m), relatively large blocks start to occur as the *S* increases to 0.04 m; however, when the *D* value is fixed at a large value (e.g., 40 m), the relatively large blocks are formed as the *S* reaches a large value (e.g., 4 m).

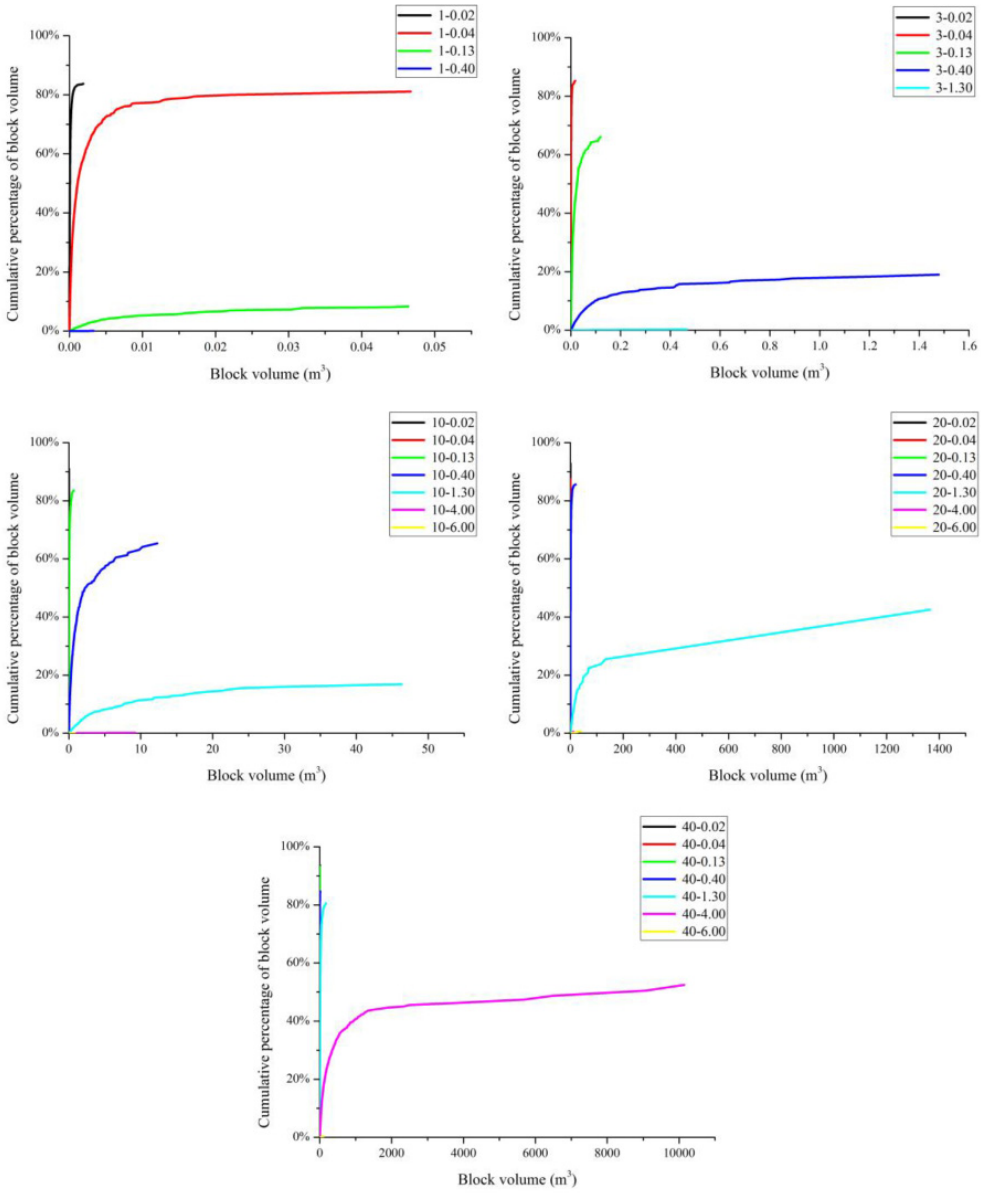

Fig. 4. Block volume curves of all models (note that in this figure, the "1-0.02" means that the model's discontinuity diameter and spacing are 1 m and 0.02 m, respectively, and is similar for the other models of this figure)

The above analyses demonstrate that when the *D* is fixed, the differences between the block volumes within the rock mass and the percentage of relatively large blocks is advanced with the growth of *S*; if *S* is fixed, the sum of the relatively small blocks within the rock mass is advanced with the growth of *D*, and the distinctions between the volumes of the blocks within the rock

mass are subsided. Table 6 and Fig. 4 show that the B_z values tally with the block scales and are also subject to the block scales and the differences between the relative volumes of the blocks within the rock mass.

5. Correlation between *Bz* and RQD/*S*

5.1. Correlation between *Bz* and RQD

To remove the direction bias, the mean RQD value was defined as the representative RQD value of a rock mass. Then, the values of *D* and *S* were fixed. Finally, by using the coefficient of variation of RQD ($C_{v\text{-RQD}}$) (i.e., the ratio of the variance of RQD to the mean RQD value, which indicates the discrete degree of the RQD values in a rock mass), the influence of the borehole direction on the RQD value and the correlation between B_z and RQD were evaluated, as shown in Fig. 5.

Fig. 5 specifically shows that B_z is well correlated with *S* and *D*. As shown in Fig. 5 (a), under the condition of a fixed *D*, and no matter how large or small it is, the B_z values tend to decrease sharply with the increase in *S*, and its largest variation range is approximately 90%, which indicates that *S* has great effects on B_z. As Fig. 5 (b) shows, a general law is that when the *S* remains unchanged, the B_z values tend to increase with the increase in *D*; however, when the *S* is fixed, especially in the range from extremely close to very close or from very wide to extremely wide, slowly increasing or invariable B_z values are experienced with the variation of *D*, which indicates that the *D* has little effect on B_z under such a circumstance. Therefore, *S* is a major factor affecting B_z, and *D* has a minor effect on B_z when the *S* value is moderate. This conclusion is similar to the previous study (Du, 1999) declaring that the discontinuity sizes have minor effects on rock mass integrity.

Fig. 5 also shows that the correlation between RQD and *S* is excellent, but the one between RQD and *D* is poor. In Fig. 5 (a), under the condition of identical *D* values, with an increased *S*, the RQD values and the $C_{v\text{-RQD}}$ increase and decrease, respectively. Moreover, the RQD changes are at least 90% or more, and when the *S* increases to a moderate value or larger, all the $C_{v\text{-RQD}}$ values are close to 0, which indicates that the degree of the influences of borehole directions on RQD values gradually decrease and the RQD values tend to homogeneity with the increase in *S*. In Fig. 5 (b), in the condition of an unchanged *S* value, the RQD values are not sensitive to the changes of *D*, and the variations of $C_{v\text{-RQD}}$ are also quite irregular. Meanwhile, when the fixed *S* is close to a small value (e.g., in the extremely to moderate range), RQD and $C_{v\text{-RQD}}$ appear to vary markedly with the increased *D*. If the *S* is fixed at a large value (e.g., in the wide to extremely wide range), RQD and $C_{v\text{-RQD}}$ tend to plateau with *D*.

Although the dimensions are completely different, B_z and RQD share features that are subject to *S*. The difference is that the *D* has a regular correlation with B_z but has no obvious influence on RQD. From the statistical analysis, the relation between B_z and RQD is as follows:

$$B_z = 1 - 0.93 \times \mathrm{RQD} \tag{5}$$

As seen in Eq. (5), the coefficient sign of RQD is negative, which means higher RQD values leads to lower B_z values. The predicted RQD values are obtained from Eq. (5), and the comparison between the measured and predicted RQD values is shown in Fig. 6.

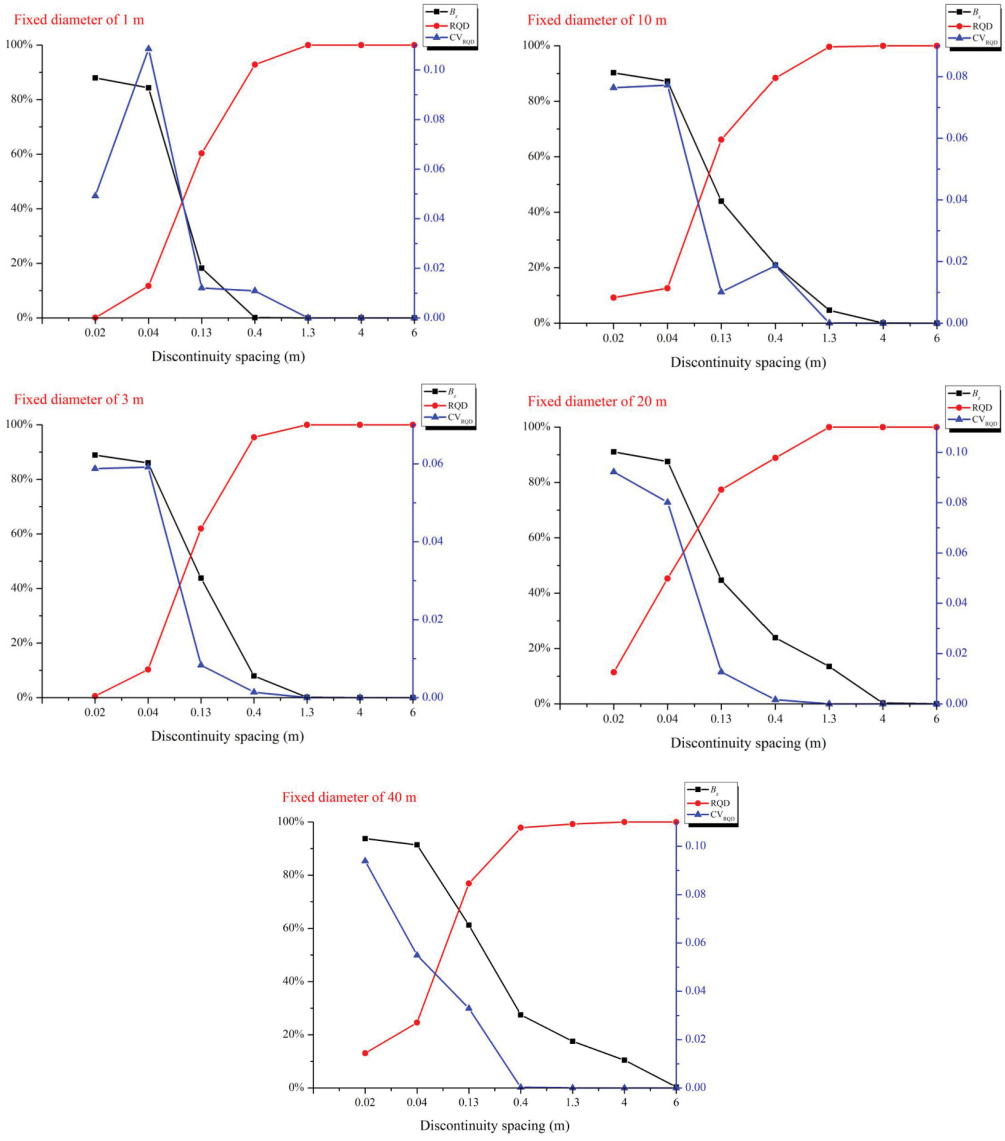

(a) Correlations between B_z and RQD under the conditions of fixed D and variable S

Fig. 5. Correlations between B_z and RQD

There is a 1:1 correlation between the measured and predicted RQD values, and the correlation coefficient (R^2) is 0.90. RQD is a one-dimensional measurement, and only counts the percentage of the sum of the lengths of core pieces longer than 10 cm to the total core run length. It is difficult to relate RQD to the other measurements of rock mass integrity (Palmstrom, 2005). In addition, B_z takes D into consideration, and it is inevitable that the correlation coefficient is not very high.

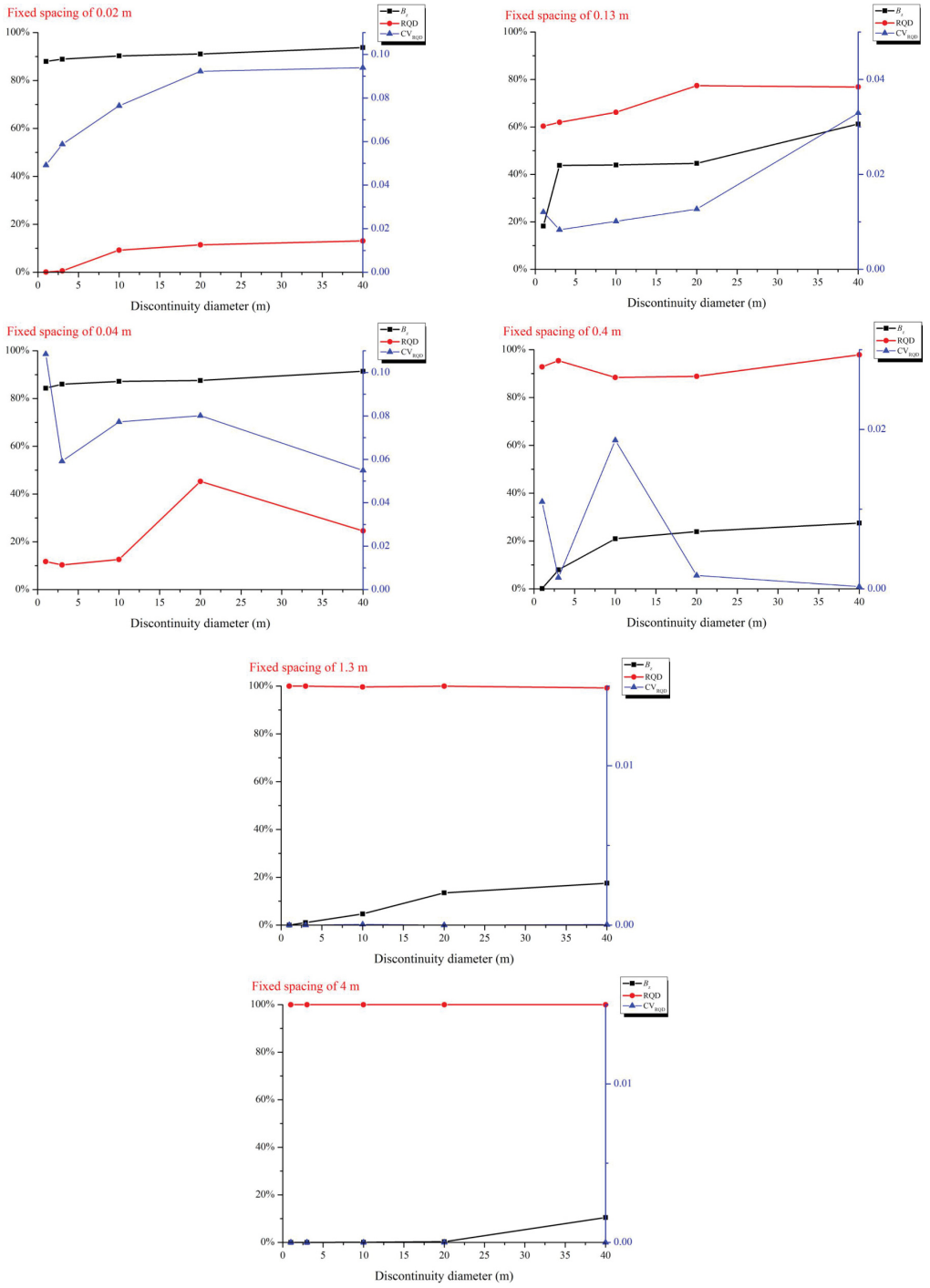

Fig. 5. Correlations between B_z and RQD

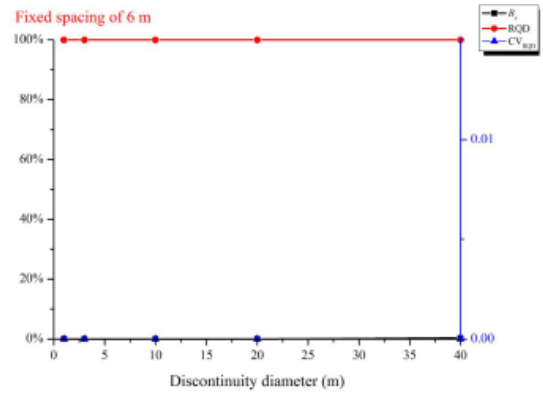

(b) Correlations between B_z and RQD under the condition of fixed S and variable D

Fig. 5. Correlations between B_z and RQD

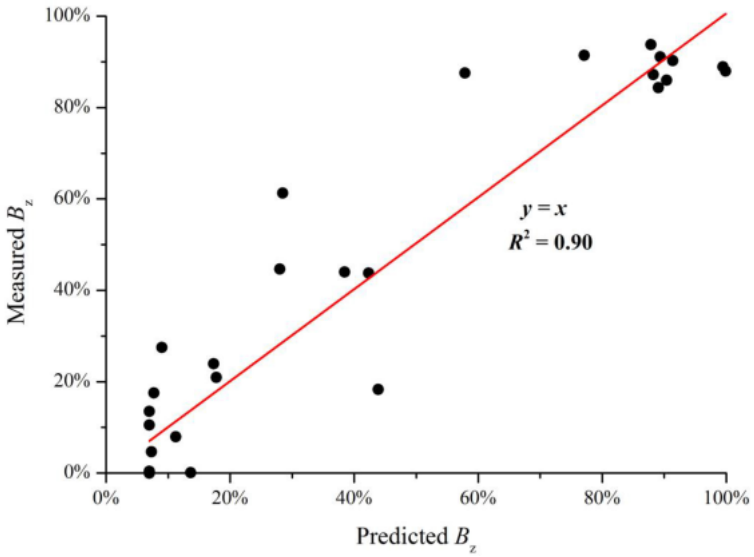

Fig. 6. Comparison of the measured B_z values and the B_z values predicted using Eq. (5)

5.2. Correlation between B_z and S

The B_z values from Table 6 are plotted with the S values from Table 3, as shown in Fig. 7. B_z has a good correlation with S, including:

(i) When the D is fixed, the B_z values decrease with the increase in S. A higher S value means a lower value of d_3, which indicates that the intersecting degree of discontinuities and the sum of the relatively large blocks within the rock mass are reduced.

(ii) If the S is fixed, the B_z values are advanced with the growth of D, especially when the S is fixed at a small value, this relation is evident.

Because there are seven grouping of models that have their own typical S values, individually. It is better to consider the S and D when evaluating the correlation between B_z and S. From the statistical analysis, the relation between B_z, S and D is as follows:

$$B_z = e^{\left(\frac{-S}{0.118+0.03\times D}\right)} \tag{6}$$

where S and D are the discontinuity spacing and diameter, respectively. As shown in Eq. (6), the coefficient sign of S is negative, which means that a higher S value leads to lower B_z values. The B_z values of the 35 types of models are estimated from Eq. (6) and are subsequently compared with the measured values, as shown in Fig. 8. A linear correlation of $y = x$ between the measured and predicted B_z values is depicted in Fig. 8, and the correlation coefficient is 0.96. This suggests that B_z is well correlated with S and D, and may be directly estimated from them.

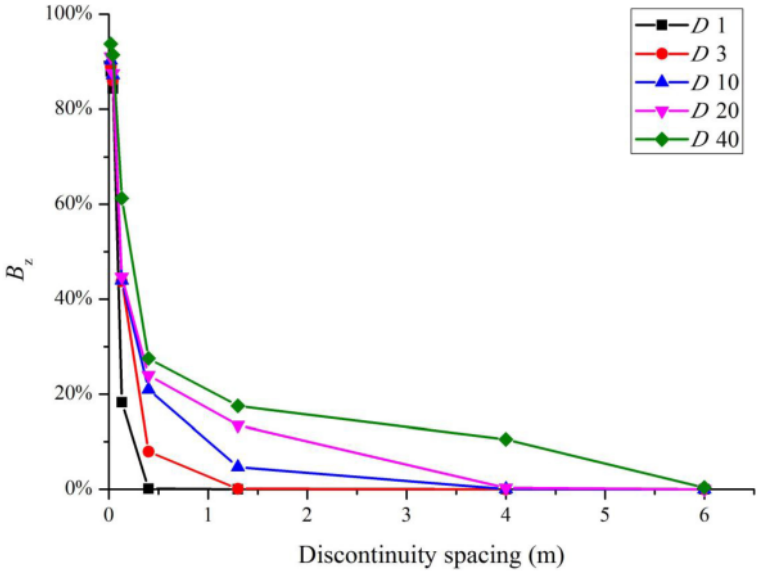

Fig. 7. Correlations between B_z and S (note that the D 1, D 3, D 10, D 20 and D 40 in this figure are the fixed discontinuity diameter values of 1 m, 3 m, 10 m, 20 m and 40 m, respectively)

S is applied in RMR system because the discontinuities intersecting in the rock mass reduce the rock mass strength and their density governs the degree of such a reduction (Bieniawski, 1989). However, S is difficult to calculate and is therefore limited under some circumstances (Palmstrom, 2005). Lowson and Bieniawski (2013) suggested using one-dimensional discontinuity density (i.e., the number of discontinuities per meter) to substitute for RQD and S. It is a change in form, but not in content. The discontinuities within rock masses intersect in three dimensions, and the one-dimensional indices (i.e., RQD, S and one-dimensional discontinuity density) lack precise estimations of the degree of rock mass fracturing.

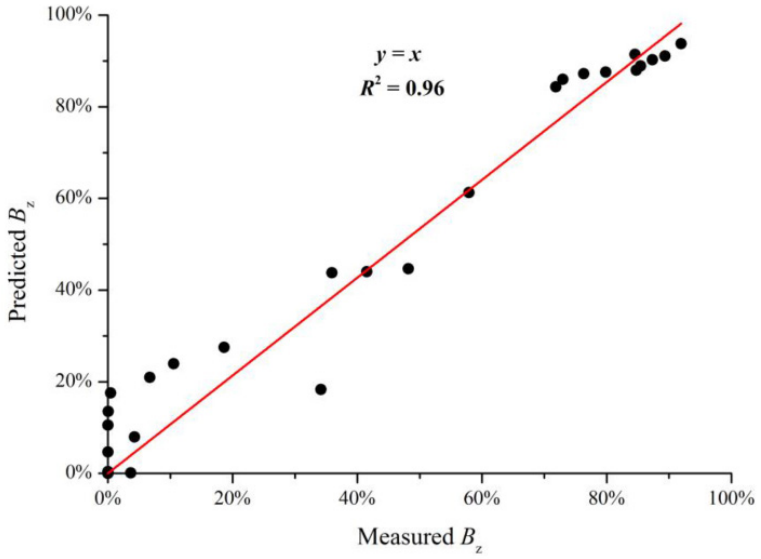

Fig. 8. Comparison of the measured B_z values and the B_z values predicted using Eq. (6)

6. Reliability of replacing RQD and *S* with B_z

The most direct way to verify the reliability of this substitution is to evaluate the relation between B_z and RQD and S. As mentioned above, B_z is different from RQD and *S* in the perspective of dimensions. In real cases, discontinuities of real three-dimensional shapes intersect within rock masses, and they possess some geometrical properties (i.e., orientation, density and size), and the discontinuity orientations were fixed in this study. Therefore, to make the dimensions consistent, *D* was considered. From the statistical analysis, a linear multiple correlation is as follows:

$$B_z = (0.00519 \times D - 0.02365 \times S - 0.87159 \times \mathrm{RQD} + 0.9229) \times 100\% \tag{7}$$

where *D* is the discontinuity diameter.

A comparison between the measured and predicted B_z values by Eq. (7) is shown in Fig. 9. As seen in the figure, the predicted values have a correlation of $y = x$ with the measured data, and a good correlation coefficient (0.96) is shown, which indicates that this correlation is reasonable. Both discontinuity density and size are taken into consideration in the modified blockiness evaluation method, and the RMR system (i.e., RQD and *S*) only focuses on discontinuity density. Comparatively, B_z is a more comprehensive and sophisticated index for evaluating the rock mass structure.

To intuitively check whether or not B_z works in RMR system, it is necessary to check the B_z ratings of the thirty-five models against the ratings of RQD and *S*. The latest version of the ratings of RQD and *S* (Warren et al., 2016) are:

$$\mathrm{V(RQD)} = 0.2 \times \mathrm{RQD} \tag{8}$$

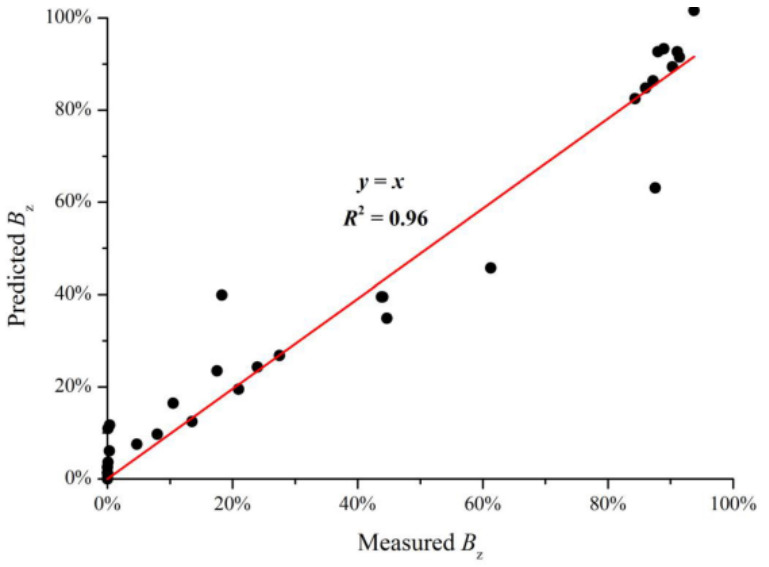

Fig. 9. Comparison of the measured B_z values and the B_z values predicted using Eq. (7)

$$V(S) = -3.767 \times \ln\left(\frac{1}{S}\right) + 16.482 \tag{9}$$

$$V(RQD + S) = V(RQD + V(S) \tag{10}$$

where V(RQD) is the score of RQD, V(S) is the score of S and V(RQD + S) is the sum of the scores of RQD plus S. Additionally, the rating of B_z is established (Table 7). A higher score indicates a smaller value of B_z and vice versa. The B_z ratings of thirty-five models are plotted against the ratings of RQD plus S, as shown in Fig. 10.

TABLE 7

Ratings for B_z

B_z (%)	< 7	7 ~ 27	27 ~ 55	55 ~ 85	≥ 85
Rating	37 ~ 40	29 ~ 37	18 ~ 29	6 ~ 18	0 ~ 6

The figure shows that the ratings of B_z have a good correlation of $y = x$ with the ratings of RQD plus S, and the correlation coefficient is 0.92, which indicates that the characterizations of the rock mass structure of B_z is similar to the ones of RQD plus S and is acceptable for engineering applications.

It is found that the B_z score of some models has some differences with the sum of the scores of RQD and S. Therefore, the models whose difference between the two scores is more than 4 points (i.e., $|V(Bz) - V(RQD + S)| > 4$) are highlighted with red points in Fig. 10, and the corresponding data are presented in Table 8.

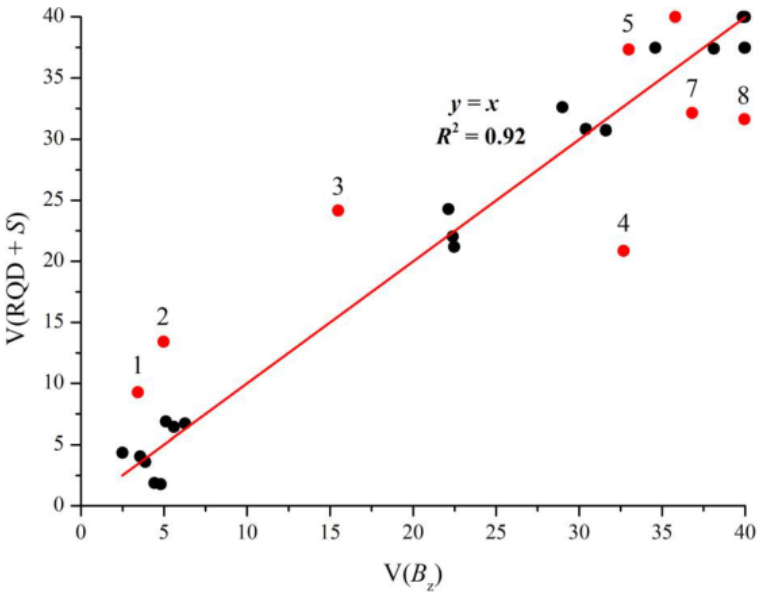

Fig. 10. Comparison between the ratings of B_z and RQD with S

TABLE 8

Data of red points in Fig. 10

Point number	B_z	V (B_z)	RQD	V (RQD)	S (m)	V (S)	V (RQD + S)	RQD	K_v	B_z
1	91.43%	3.43	24.60%	4.92	0.04	4.36	9.28	Very poor (V)	Fractured (V)	Serious-blockiness (V)
2	87.56%	4.98	45.31%	9.06	0.04	4.36	13.42	Poor (IV)	Fractured (V)	Serious-blockiness (V)
3	61.27%	15.49	76.88%	15.38	0.13	8.80	24.18	Good (II)	Relatively fractured (IV)	Blockiness (IV)
4	18.28%	32.68	60.34%	12.07	0.13	8.80	20.87	Fair (III)	Relatively integrated (II)	Slight-blockiness (II)
5	17.54%	32.98	99.25%	19.85	1.3	17.47	37.32	Excellent (I)	Relatively integrated (II)	Slight-blockiness (II)
6	10.50%	35.8	100%	20	4	20	40	Excellent (I)	Relatively integrated (II)	Slight-blockiness (II)
7	7.97%	36.81	95.44%	19.09	0.4	13.03	32.12	Excellent (I)	Relatively integrated (II)	Slight-blockiness (II)
8	0.11%	40	92.85%	18.57	0.4	13.03	31.60	Excellent (I)	Integrated (I)	Non-blockiness (I)

As seen in Table 8, the combined use of RQD and S has several limitations, including:

(i) With the exception of models No. 1 and No. 8, the characterizations of the models' RQD ratings do not match with the ones of the ratings of B_z and K_v (Liu et al. 2017), especially for model No. 3, its RQD description and rating are good and in class II, respectively, but the ratings of B_z and K_v show a blockiness and poorly integrated rock mass. The RQD rating deviates from the actual.

(ii) The ratings of RQD plus S overrates the structure of poor rock mass. As seen in Fig. 10, most of the sums of the scores of RQD plus S in poor rock mass are higher than the scores of B_z. Maybe that is why the RMR system does not work well at weak rock mass, and its evaluations for weak rock mass are too high (Aksoy, 2008; Warren et al., 2016). Additionally, in view of the ratings of B_z and K_v, models No. 1 to No. 3 are poor rock mass from the perspective of rock mass structure; however, their scores of RQD plus S are higher than the B_z scores. Therefore, the final RMR values may too high for weak rock mass.

(iii) For the models whose qualities and integrities are fair or better (e.g., the models No. 4 to No. 8), the differences between the B_z scores and the scores of RQD plus S are in the range from 4 to 5 and, therefore, are barely satisfactory except for models No. 4 and No. 8. For models No. 4 and No. 8, their ratings of RQD, B_z and K_v indicate that the rock mass is integrated. The ratings of RQD plus S are too low due to the low scores of S. Actually, according to the classification standard of S, the low scores are deserved, while it shows that the S, an index of one-dimensional discontinuity density, is limited under some circumstances.

As shown in Tables 4 and 8 and Fig. 4, the degree of rock mass fracturing and the effect of block dimensions are considered in the modified blockiness evaluation method. Different B_z values characterize different rock mass structures and block distributions. The B_z values emphasize the integrity differences between different structural rock masses and make the evaluation of the rock mass structure more accurate, and therefore, the use of B_z in rock mass classification is acceptable.

The above analyses show that the relation between B_z, RQD, S and D is good, and a $y = x$ correlation between the scores of B_z and RQD plus S is evaluated in Fig. 10. It illustrated that B_z can be used as a direct replacement of the combined used of RQD and S in the RMR system. Meanwhile, because of the limitations of RQD and because the scores of RQD plus S are higher than the actual for weak rock mass, sometimes the ratings of RQD plus S are not in agreement with the actual rock mass structure. B_z is more sensitive to the block distribution dominating the rock mass integrity, as seen in Fig. 4, Tables 6 and 8.

7. Applications to real cases

7.1. Study areas

Tongkeng Mine is located in Nandan County (Guangxi Province, China), forty-six kilometers north of Nandan County Town, and eighty-four kilometers east of Hechi City (Fig. 11). The aerial view of Tongkeng Mine is shown in Fig. 12. Tongkeng Mine is an enterprise belonging to the Huaxi Group of Guangxi (China), with a yearly production capacity of 220×104 tons. There are

three large ore bodies that have been discovered in Tongkeng Mine, i.e., Veinlet Belt orebody, No. 91 orebody and No. 92 ore body. The first two ore bodies were depleted, and the No. 92 ore body is being mined now.

Fig. 11. Map of the Tongkeng Mine (China)

Fig. 12. Ariel view of the Tongkeng Mine

The rock masses of the No. 92 ore body are mainly of silicalite, which is harder. Well-developed discontinuities occur in some parts of the ore body and therefore lead to roof failures, collapses, and secondary disasters after strengthening countermeasures have been taken. Four study areas in different levels were chosen to perform the applications of the RMR systems following the standard approach and using B_z, as shown in Fig. 13. The results of the discontinuity investigation at the four study areas are presented in Fig. 14 and Table 9. Furthermore, in all the study areas, 91 percent of the discontinuity belongs to the medium category, and the rest are in very low, low and high categories.

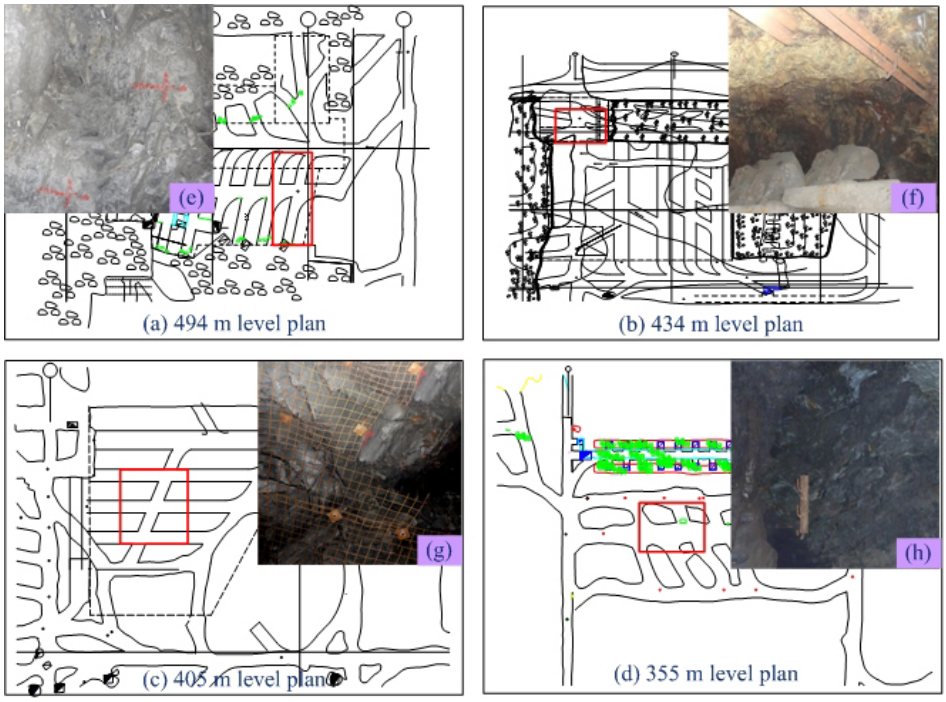

Fig. 13. Locations of the study areas and their rock mass observations. (a), (b), (c) and (d) are the planimetric locations of the A1, A2, A3 and A4 areas, respectively; (e), (f), (g) and (h) are the observations of the rock masses in the A1, A2, A3 and A4 areas, respectively

TABLE 9

Distributions of the critical discontinuity sets at different sites

Site	Dip direction interval	Discontinuity number	Average dip/dip direction	Discontinuity frequency
A1	10 ~ 30	119	63.6/17.9	0.22
	30 ~ 50	130	45.8/35.1	0.24
A2	10 ~ 30	71	42/20	0.63
	100 ~ 120	24	65.1/110.4	0.21
A3	320 ~ 350	339	20/335	0.79
A4	180 ~ 200	171	25/190	0.75
	210 ~ 230	48	32/220	0.21

7.2. RMR values calculated following the standard approach and using *Bz*

Based on the results of the discontinuity investigation, geological survey and rock mass mechanical test, the rock masses of the study areas were evaluated according to the standard RMR system, as shown in Table 10. The table shows that the rock mass quality of the A3 area is the worst, and the rest are almost identical.

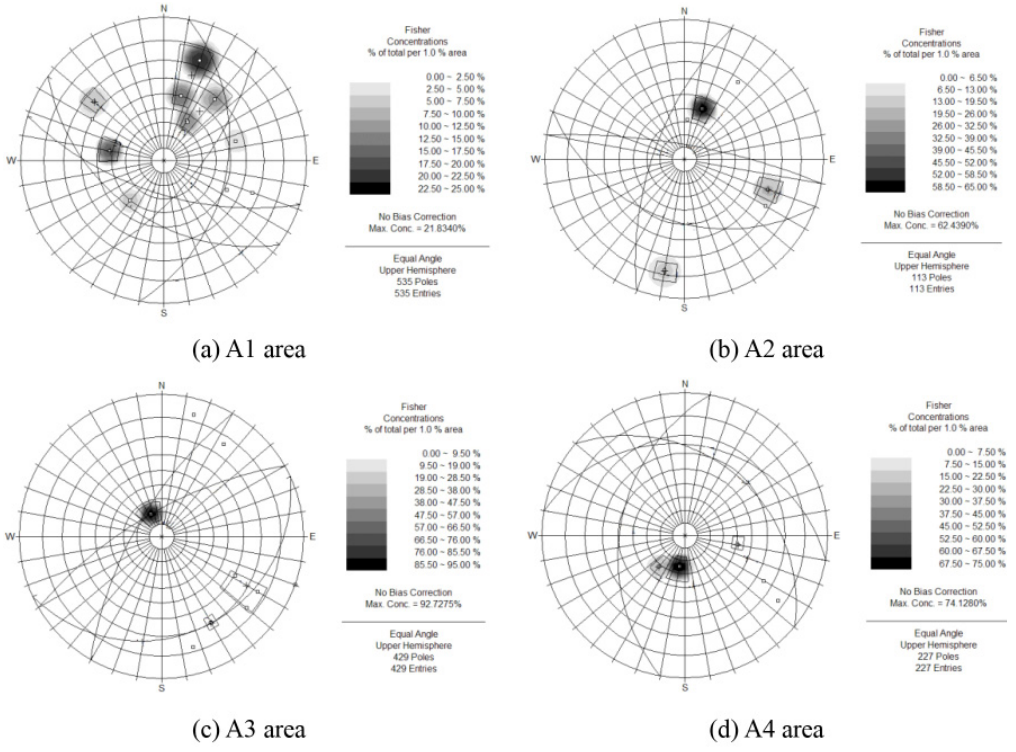

Fig. 14. Contour plots of the discontinuity poles collected from the four test areas

TABLE 10

RMR scores of the four areas of the No. 92 orebody

Site \ Parameters		*UCS*	RQD	Discontinuity spacing	Discontinuity condition	Ground water	Total score	Rating
A1	Parameters description	81 MPa	28.7%	8.7 cm	Separation < 0.1 cm, slickensided surfaces, high persistence	Completely dry	48	III
	Score	7	8	8	10	15		
A2	Parameters description	82 MPa	69.5%	15 cm	Separation < 1 mm, slightly rough surface, low persistence	Dripping	42	III
	Score	7	13	8	10	4		
A3	Parameters description	85 MPa	40.6%	15 cm	Separation < 5 mm, slickensided surface, high persistence	Dripping	32	IV
	Score	7	8	8	5	4		
A4	Parameters description	79 MPa	28.7%	5.7 cm	Undeveloped joints, separation < 1 mm, medium persistence	Dripping	43	III
	Score	7	8	5	20	4		

The calculations of the B_z values are usually based on the DFN model of the rock mass. In these cases, the process of building the discontinuity network models is different from the conventional method of generating the DFN model of the rock mass. In these cases, sufficient outcrops in different locations and directions are available owing to the excavation of stop structure, the three-dimensional discontinuity network models of the four study areas can be directly established by the deterministic discontinuity data collected from the areas rather than the stochastic discontinuities generated by the Mote-Carlo simulation method. It is noted that if available outcrops are scarce, DFN is the only way to build the three-dimensional discontinuity network model of the rock mass.

Considering the influences of Representative Elementary Volume (REV) (Xia et al., 2016), the three-dimensional discontinuity network models of the A1 to A4 areas were generated by GeneralBlock, with dimensions of 4 m×4 m×4 m, 4.5 m×4.5 m×4.5 m, 6.5 m×6.5 m×6.5 m and 5 m×5 m×5 m, respectively (Fig. 15). The B_z values of all models were calculated through the block volume data generated by General Block, and the RMR values computed using B_z were obtained, as shown in Table 11. The table shows that the rock mass quality of the A3 area is in class V (the worst one), with a blockiness level category of serious-blockiness, indicating

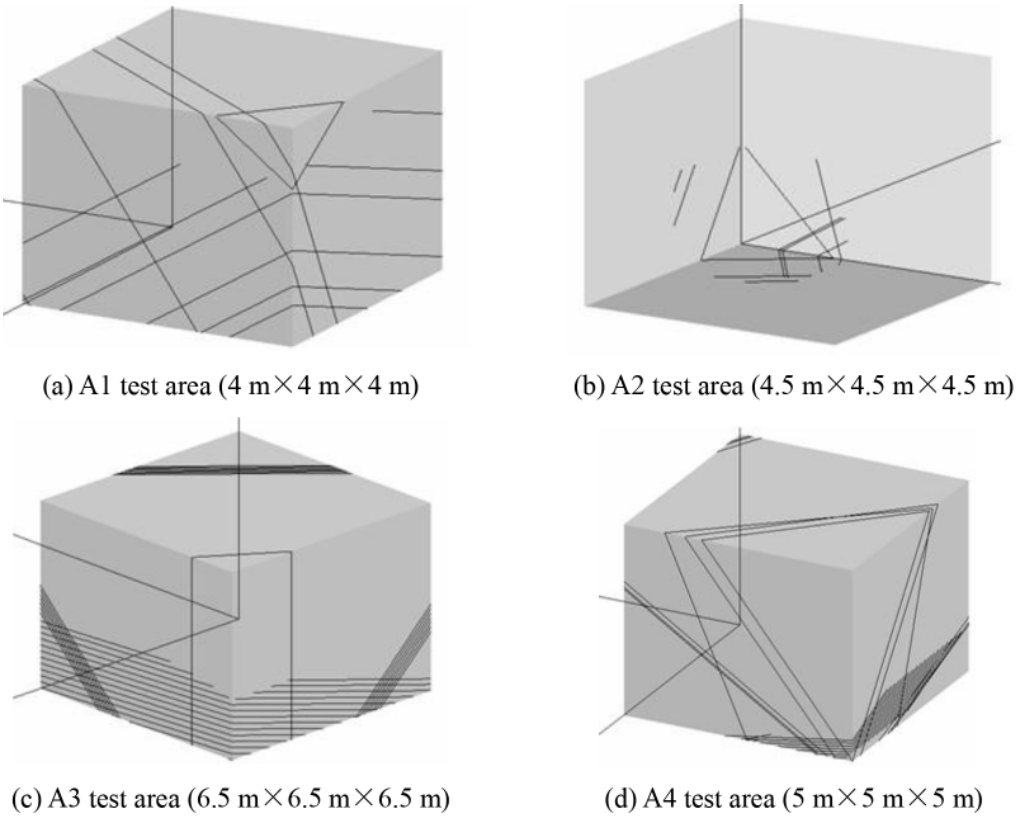

Fig. 15. Three-dimensional discontinuity network models of the rock masses at the four areas (note that due to the graphics blanking, some discontinuities are not observable)

the intactness degree of the rock mass is very low, and it is consistent with the outcomes of the standard RMR system; the rock mass of the A4 area is the best and belongs to the good category (II), and the degree of rock mass fracturing is very low, with a B_z value of 16.3%. The RMR values based on the B_z method fully reflect that the rock mass qualities and behaviors are primarily subject to the rock mass structures.

TABLE 11

B_z and RMR values of the rock masses at the four areas

Site	B_z	Classification of B_z	B_z value	RMR values calculated using B_z	RMR value calculated following standard approach
A1	62.25%	Blockiness rock mass	15.12	47.12 (III)	48 (III)
A2	74.9%	Blockiness rock mass	10.04	31.04 (IV)	42 (III)
A3	92.04%	Serious-blockiness rock mass	3.18	19.18 (V)	32 (IV)
A4	16.3%	Slight-blockiness rock mass	33.48	64.48 (II)	43 (III)

7.3. Comparisons between the two approaches

In underground mine applications, the easiest and most direct way to verify the rock mass classification results is to observe the drive where the work is being done (Potvin et al., 2012). In the practical project (Fig. 13), the roof of the A1 area is relatively stable, but rock falls occasionally occur; in the A2 area, rock stratum falls occur in some places, and anchor bolt supports are implemented; in A3 area, the rock masses are very fractured, the roofs are extremely instable, large inbreaks continually occur when excavating, and it requires the implementation of the anchor network supports after the roadway forms; in the A4 area, the rock masses are very integrated, and the roof is very stable, so there is no need for additional support. According to the actual conditions of the areas, the characterizations of the B_z method are in agreement with the practices, which are capable of distinguishing the rock mass intactness degrees at different study areas.

Table 11 shows a comparison between the two approaches, indicating that there is a difference between the RMR systems based on the standard approach and the B_z method. For the A1 area, the RMR assessments using the two approaches all belong to the fair category, and in practice, only some rock collapses of uneven sizes occur in the A1 area, therefore, only wall tapping and roof sounding are implemented to meet the security requirements. It also demonstrates that the abilities of the two approaches to assess rock mass quality are similar when the rock masses are in the fair category. For A2 area, the RMR evaluation using B_z is poor, while the one following standard approach is fair, but in the field, rock stratum falls occur in some parts of the A2 area, reflecting a poorer rock mass quality. For the A3 area, the classification using the standard RMR system indicates a rock mass quality in class IV, while the one based on B_z shows it in class V. The practical situation of the field is that the anchor network supports are immediately implemented when the roadway shape forms, otherwise roof failures occur. At this point, class V with an average stand-up time description of 30 min for a 1 m span is more accurate. For the A4 area, the RMR value computed through the standard method is in the fair category, while the value obtained by B_z is in the good category. In the field, there is no need to add support in the A4 area, because the roofs remain stable after the excavation.

Tables 10 and 11 shows that, for the rock masses with higher fracturing degrees (e.g., A2 and A3 areas), the combined use of RQD and S may provide a biased description of the rock mass structure in reality, which validates the above-mentioned theoretical analyses (Fig. 10 and Table 8). The comparisons reveal that the B_z, whose abilities to characterize rock mass structures are higher than the combined use of RQD and S, could recognize the distinctions of the rock mass intactness degrees between various rock masses, and therefore, the RMR values calculated through B_z are more in line with the actual situations.

8. Conclusions

Evaluations of the rock mass structure in RMR systems (i.e., RQD and S) are limited and therefore inaccurate under some circumstances. The authors put forward an idea that uses B_z to replace RQD and S. To investigate its reliability, thirty-five theoretical DFN models with different structures were built and their RQD and B_z values were calculated. Subsequently, the correlations between B_z, RQD and S were explored, including the following:

(i) There are some uncertainties in the combined use of RQD and S. RQD values are one-dimensional discontinuity data, sometimes there are inaccuracies in RQD to characterize the rock mass integrity. Meanwhile, RQD is mainly dominated by S. The rock mass with closer S has a higher RQD heterogeneity, and its RQD values are more influenced by borehole directions.

(ii) B_z has good correlations with RQD, S and D, individually. However, RQD and S only emphasize one-dimensional discontinuity densities and ignore the effect of block dimensions. Comparatively, B_z is more comprehensive for evaluating rock mass structure.

(iii) A good correlation between B_z and the three parameters (i.e., RQD, S and D) are presented to directly guarantee the feasibility of replacing RQD and S with B_z. Additionally, by comparing the B_z and RQD plus S ratings of the thirty-five models, it is found that the combined use of RQD and S may be an inaccurate measure for rock mass structures under some circumstances, due to the inherent limitations. B_z characterizes the degree of rock mass fracturing from the perspective of block distribution and, therefore, can distinguish between different structural rock masses.

(iv) The applications and comparisons show that the standard RMR system does not suffice for the classification of the rock mass of poor quality. The B_z method enables the characterization of the rock mass fracturing degree to be more proximate to the practical situation, and therefore, the RMR values calculated using B_z are, also.

Therefore, the authors feel that B_z, a more comprehensive index, should be employed in rock mass classifications, such as the RMR system, and one-dimensional characterizations for the degree of rock mass fracturing, such as RQD and S, should be phased out.

Acknowledgements

This work was financially supported by the National Science Foundation for Young Scientists of China (Grant No. 41402306) and the Open Research Fund of State Key Laboratory of Geomechanics and Geotechnical Engineering, Institute of Rock and Soil Mechanics, Chinese Academy of Sciences (Grant No. Z016015).

References

Aksoy C.O., 2008. *Review of rock mass rating classification: Historical developments, applications, and restrictions*. J. Min. Sci. **44**, 1, 51-63. doi:10.1007/s10913-008-0005-2.

Atr J.S., Laubscher H., 2001. *A geomechanics classification system for the rating of rock mass in mine design*. J. South African Inst. Min. Metall. **90**, 10, 257-273. doi:10.1016/0148-9062(91)90830-F.

Bieniawski Z.T., 1973. *Engineering classification of jointed rock masses*. Trans. S. Afr. I. Civil Eng. **15**.

Bieniawski Z.T., 1989. *Engineering rock mass classifications: a complete manual for engineers and geologists in mining, civil, and petroleum engineering*.

Chen D.J., Liu H.T., 1979. *A new index of rock mass quality evaluation: blockiness modulus*. In: Chinese first selection of engineering geological academic conference papers. Soochow, 1979 (in Chinese).

Chen J., Li X., Zhu H., 2017. *Geostatistical method for predicting RMR ahead of tunnel face excavation using dynamically exposed geological information*. Eng. Geol. 2017. doi:10.1016/j.enggeo.2017.08.004.

Du S.G., 1999. *Engineering properties of rock mass discontinuities*. Seismological Press, Beijing (in Chinese).

Eissa E.A., 1991. *Volumetric Rock Quality Designation*. J. Geotech. Eng. **117**, 9, 1331-1346.

Elmouttie M.K., Poropat G.V., 2012. *A method to estimate in situ block size distribution*. Rock Mech. Rock Eng. **45**, 3, 401-407. doi:10.1007/s00603-011-0175-0.

Ferrari F., Apuani T., Giani G.P., 2014. *Rock Mass Rating spatial estimation by geostatistical analysis*. Int. J. Rock Mech. Min. Sci. **70**, 162-176. doi:10.1016/j.ijrmms.2014.04.016.

González Nicieza C., Álvarez Fernández M.I., Menéndez Díaz A., Álvarez Vigil A.E., 2006. *Modification of rock failure criteria considering the RMR caused by joints*. Comput. Geotech. **33**, 8, 419-431. doi:10.1016/j.compgeo.2006.08.004.

Hoek E., Diederichs M.S., 2013. *Quantification of the Geological Strength Index Chart*. 47th US Rock Mech. / Geomech. Symp. held San. Fr. CA, USA, June 23-26.

Hoseinie S.H., Aghababaei H., Pourrahimian Y., 2008. *Development of a new classification system for assessing of rock mass drillability index (RDi).* Int. J. Rock Mech. Min. Sci. **45**, 1, 1-10. doi:10.1016/j.ijrmms.2007.04.001.

ISRM, 1978. *Suggested methods for the quantitative description of discontinuities in rock masses*. Int. J. Rock Mech. Min. Sci. Geomech. Abstr. **15**, 319-368. doi:10.1016/0148-9062(79)91476-1.

Jain P., Naithani A.K., Singh T.N., 2016. *Estimation of the performance of the tunnel boring machine (TBM) using uniaxial compressive strength and rock mass rating classification (RMR) – A case study from the Deccan traps, India*. J. Geol. Soc. India **87**, 2, 145-152. doi:10.1007/s12594-016-0382-0.

Jalalifar H., Mojedifar S., Sahebi A.A., 2014. *Prediction of rock mass rating using fuzzy logic and multi-variable RMR regression model*. Int. J. Min. Sci. Technol. **24**, 2, 237-244. doi:10.1016/j.ijmst.2014.01.015.

Jalalifar H., Mojedifar S., Sahebi A.A., Nezamabadi-pour H., 2011. *Application of the adaptive neuro-fuzzy inference system for prediction of a rock engineering classification system*. Comput. Geotech. **38**, 6, 783-790. doi:10.1016/j.compgeo.2011.04.005.

Justo J.L., Justo E., Azanon J.M., Durand P., Morales A., 2010. *The use of rock mass classification systems to estimate the modulus and strength of jointed rock*. Rock Mech. Rock Eng. **43**, 3, 287-304. doi:10.1007/s00603-009-0040-6.

Khademi J., Shahriar K., Rezai B., Rostami J., 2010. *Performance prediction of hard rock TBM using Rock Mass Rating (RMR) system*. Tunn. Undergr. Sp. Technol. Inc. Trenchless. Technol. Res. **25** 4, 333-345. doi:10.1016/j.tust.2010.01.008.

Kuszmaul J.S., 1999. *Estimating keyblock sizes in underground excavations: accounting for joint set spacing*. Int. J. Rock. Mech. Min. Sci. **36**, 2, 217-232. doi:10.1016/S0148-9062(98)00184-3.

Li P.F., Yang J.H., Nie D.X., 2009. *Study on Modification of Volumetric Joint Count*. J. Yangtze River. Sci. Res. Inst. **26**, 12, 80-83 (in Chinese with English abstract).

Li S.C., Liu H., Li L.P., et al., 2017. *A quantitative method for rock structure at working faces of tunnels based on digital images and its application*. Chin. J. Rock Mech. Eng. **36**, 1, 1-9 (in Chinese with English abstract).

Li X.C., Rui X.P., Qu X.K., et al., 2016. *Algorithm of karst fracture seepage path construction based on disc generalized model*. J. Geo. Inform. Sci. **18**, 2, 182-189. doi:10.3724/SP.J.1047.2016.00182 (in Chinese with English abstract).

Liu J., Elsworth D., Brady B.H., 1999. *Linking stress-dependent effective porosity and hydraulic conductivity fields to RMR*. Int. J. Rock Mech. Min. Sci. **36**, 5, 581-596. doi:10.1016/S0148-9062(99)00029-7.

Liu Q., Liu J., Pan Y., et al., 2017. *A case study of TBM performance prediction using a Chinese rock mass classification system – Hydropower Classification (HC) method*. Tunn. Under. Sp. Tech. **65**, 140-154.

Liu X.F., 2010. *Study on blockiness of fractured rock mass*. Dissertation, China University of Geosciences (Beijing) (in Chinese with English abstract).

Liu Z. xiang, Dang W. gang, 2014. *Rock quality classification and stability evaluation of undersea deposit based on M-IRMR*. Tunn. Undergr. Sp. Technol. **40**, 95-101. doi:10.1016/j.tust.2013.09.013.

Lowson A.R., Bieniawski Z.T., 2013. *Critical Assessment of RMR based Tunnel Design Practices: a Practical Engineer's Approach*. Rapid Excav. Tunneling Conf. (June), 16.

Mutlu B., Sezer E.A., Nefeslioglu H.A., 2017. *A defuzzification-free hierarchical fuzzy system (DF-HFS): Rock mass rating prediction*. Fuzzy Sets. Syst. **307**, 50-66. doi:10.1016/j.fss.2016.01.001.

Nikafshan Rad H., Jalali Z., Jalalifar H., 2015. *Prediction of rock mass rating system based on continuous functions using Chaos-ANFIS model*. Int. J. Rock Mech. Min. Sci. **73**, 1-9. doi:10.1016/j.ijrmms.2014.10.004.

Niu W.J., 2017. *Study on the modification of blockiness evaluation method and the geometric and mechanical effect of fractured rock mass*. Dissertation, Guangxi University (in Chinese with English abstract).

Palmstrom A., 2005. *Measurements of and correlations between block size and rock quality designation (RQD).* Tunn. Undergr. Sp. Technol. **20**, 4, 362-377. doi:10.1016/j.tust.2005.01.005.

Palmström A., 2009. *Combining the RMR, Q, and RMi classification systems*. Tunn. Undergr. Sp. Technol. **24**, 4, 491-492. doi:10.1016/j.tust.2008.12.002.

Paul A., Singh A.P., Loui P.J., Singh A.K., Khandelwal M., 2012. *Validation of RMR-based support design using roof bolts by numerical modeling for underground coal mine of Monnet Ispat, Raigarh, India – a case study*. Arab. J. Geosci. **5**, 6, 1435-1448. doi:10.1007/s12517-011-0313-8.

Pells P., Bieniawski Z.T.R., Hencher S., Pells S., 2016. *RQD: Time to Rest in Peace*. Can. Geotech. J. (1974):cgj - 2016-0012. doi:10.1139/cgj-2016-0012.

Pinheiro M., Emery X., Miranda T., Vallejos J., 2016. *Truncated Gaussian Simulation to Map the Spatial Heterogeneity of Rock Mass Rating*. Rock Mech. Rock Eng. **49**, 8, 3371-3376. doi:10.1007/s00603-016-0928-x.

Pinheiro M., Vallejos J., Miranda T., Emery X., 2016. *Geostatistical simulation to map the spatial heterogeneity of geomechanical parameters: A case study with rock mass rating*. Eng. Geol. **205**, 93-103. doi:10.1016/j.enggeo.2016.03.003.

Potvin Y., Dight P.M., Wesseloo J., 2012. *Some pitfalls and misuses of rock mass classification systems for mine design.* J. S. Afr. I. Min. Metall. **112**, 8, 697-702.

Priest S.D., 1993. *Discontinuity analysis for rock engineering*. Chapman & Hall, London.

Romana M., 1993. *A Geomechanical Classification for Slopes: Slope Mass Rating*. Compr. Rock Eng. 575-599. doi:http://dx.doi.org/10.1016/B978-0-08-042066-0.50029-X.

Ruf J.C., Rust K.A., Engelder T., 1998. *Investigating the effect of mechanical discontinuities on joint spacing*. Tectonophysics **295**, 1-2, 245-257. doi:10.1016/S0040-1951(98)00123-1.

Ruiz-Carulla R., Corominas J., Mavrouli O., 2015. *A methodology to obtain the block size distribution of fragmental rockfall deposits*. Landslides **12**, 4, 815-825. doi:10.1007/s10346-015-0600-7.

Şen Z., Bahaaeldin B.H., 2003. *Modified rock mass classification system by continuous rating*. Eng. Geol. **67**, 3-4, 269-280. doi:10.1016/S0013-7952(02)00185-0.

Sereshki F., Daftaribesheli A., Ataei M., 2010. *A mamdani fuzzy inference system for rock mass rating (RMR) and its use in rock mass parameters estimation*. Arch. Min. Sci. **55**, 4, 947-960.

Shi G.H., 2006. *Producing joint polygons, cutting joint blocks and finding key blocks for general free surfaces*. Chin. J. Rock Mech. Eng. **25**, 11, 2161-2170.

Stavropoulou M., 2014. *Discontinuity frequency and block volume distribution in rock masses*. Int. J. Rock Mech. Min. Sci. **65**, 62-74. doi:10.1016/j.ijrmms.2013.11.003.

Wang C.Y., Hu P.L., Sun W.C., 2010. *Method for evaluating rock mass integrity based on borehole camera technology*. Rock Soil. Mech. **31**, 4, 1326-1330 (in Chinese with English abstract).

Wang L.H., Li J.R., Li J.L., et al., 2013. *Correction of RMR system and its engineering application*. Chin. J. Rock Mech. Eng. **32**, 3309-3316 (in Chinese with English abstract).

Wang S.C., He F.L., Li C.S., 2007. *Tunneling Rock Mass Classification*. China Southwest Jiaotong University Press, Chengdu (in Chinese).

Wang X.M., 2013. *Study on rock fractures and rock blocks in Wudongde dam area*. Disssertation, China University of Geoscience (Beijing) (in Chinese with English abstract).

Warren S.N., Kallu R.R., Barnard C.K., 2016. *Correlation of the Rock Mass Rating (RMR) System with the Unified Soil Classification System (USCS): Introduction of the Weak Rock Mass Rating System (W-RMR).* Rock Mech. Rock Eng. **49**, 11, 4507-4518. doi:10.1007/s00603-016-1090-1.

Xia L., Li M., Chen Y., Zheng Y., Yu Q., 2015. *Blockiness level of rock mass around underground powerhouse of Three Gorges Project*. Tunn. Undergr. Sp. Technol. **48**, 67-76.

Xia L., Zheng Y., Yu Q., 2016. *Estimation of the REV size for blockiness of fractured rock masses*. Comput. Geotech. **76**, 83-92. doi:10.1016/j.compgeo.2016.02.016.

Yang Z.Y., Chen J.M., Huang T.H., 1998. *Effect of joint sets on the strength and deformation of rock mass models*. Int. J. Rock Mech. Min. Sci. **35**, 1, 75-84. doi:10.1016/S1365-1609(98)80024-5.

Yu Q., Ohnishi Y., Xue G., Chen D., 2009. *A generalized procedure to identify three-dimensional rock blocks around complex excavations*. Int. J. Numer Anal. Methods Geomech. **33**, 3, 355-375. doi:10.1002/nag.720.

Zhang Q.H., Bian Z.H., Yu M.W., 2009. *Preliminary research on rock mass integrity using spatial block identification technique*. Chin. J. Rock Mech. Eng. **28**, 507-515 (in Chinese with English abstract).